This article has been accepted for publication in IEEE Transactions on Energy Conversion. This is the author's version which has not been fully edited and content may change prior to final publication. Citation information: DOI 10.1109/TEC.2024.3365353

Data-Driven Nonlinear Model Predictive Control for Power Sharing of Inverter-based Resources

Maral Shadaei, *Member, IEEE,* Javad Khazaei, *Senior Member, IEEE*, and Faegheh Moazeni, *Associate Member, ASCE*

***Abstract*—Model predictive control (MPC) is a closed-loop optimization framework that can solve the real-time control challenges of inverter-based distributed energy resources (DERs) in smart grids. This paper addresses the challenge of heavy reliance of model predictive controllers on physics-based dynamic models by proposing a data-driven MPC framework via sparse regression (SR) theory and nonlinear model predictive control (NLMPC) framework. Unlike existing approaches that rely on approximate models based on physical principles or experiments, the proposed framework directly captures the dynamics of the DERs using measurements. This capability enables power sharing among DERs and active/reactive load support with high precision. The framework can capture uncertainties and drift dynamics of DERs by updating the data-driven model on a timely manner for running the MPC for effective power sharing. By employing this approach, the overall effectiveness of active and reactive power sharing is enhanced without compromising voltage and frequency control. The proposed optimal control strategy is validated through real-time simulations conducted on a 3-DER microgrid (MG) using OPAL-RT. The results demonstrate the successful estimation of DER dynamics using the SR method and accurate power sharing through NLMPC. Furthermore, NLMPC not only achieves a high degree of precision in power tracking but also outperforms other MPC strategies that rely on successive linearization, with a mean absolute percentage error (MAPE) of 6.83% for active power and 5.71% for reactive power.**

***Index Terms*—Predictive control, Distributed energy resources (DERs), Sparse regression (SR), Nonlinear model predictive control (NLMPC), Power sharing.**

I. Introduction

THE pursuit of carbon neutrality by 2050 has intensified the shift from conventional energy sources to renewable energy resources, with DERs playing a pivotal role in this energy transition. MGs are at the vanguard of this shift, emerging as a promising means to seamlessly integrate DERs with existing distribution networks, thereby enhancing the resilience and sustainability of the energy supply [1].

To maintain effective control within an MG, it is crucial to adhere to operational constraints, necessitating the design of an advanced multi-variable control approach. Traditionally, MG operations have relied on a three-tier hierarchical control structure that includes primary, secondary, and tertiary controllers [2]. However, the dynamics of MGs and the complexity of integrating various energy sources call for more sophisticated control strategies. Table I presents a comparison of Proportional-Integral (PI), Neural Network (NN)-based, and NLMPC approaches for MG energy management. PI controllers, while simple and robust for certain applications, do not inherently handle nonlinear models or constraints and lack optimal control capabilities [3]. NN-based controllers can manage nonlinearities effectively through learned behaviors from historical data; however, they are not intrinsically designed for handling constraints or optimizing control actions. Their efficiency in these areas heavily depends on the extent and diversity of the data they have been trained on, without which their ability to satisfy operational constraints and achieve optimal performance may be compromised [4], [5]. The proposed MPC excels in managing MG energy systems by proficiently handling nonlinearities, constraints, and optimizing control. It ensures reliable power distribution for both active (P) and reactive (Q) demands and is adept at operating within complex multi-input and multi-output (MIMO) environments. The predictive nature of MPC, which forecasts and adjusts to future system changes, significantly bolsters the system's adaptability and resilience, making it a robust solution for the dynamic challenges in MG management. [6], [7].

Several studies, including those conducted by [8], [9], [10], [11], have identified the potential of MPC for enabling effective secondary control in microgrids. Authors in [8], proposed MPC approach to ensure frequency stability in low inertia power systems. In [9], a decentralized control approach utilizing MPC with V-I droop method to enhance power quality in MG is presented. What is more, [10], introduces a decentralized control strategy for multiple DGs by integrating a voltage controller using MPC with a rapid current controller utilizing discrete-time sliding-mode control to manage inverter currents during overload situations. A centralized control system for MGs, coordinating DERs through MPC algorithm that optimizes steady-state and transient control separately, while also implementing an energy management system to coordinate load sharing is introduced in [11]. While these approaches demonstrate accurate steady-state tracking and exhibit robust and fast transient characteristics, they have not fully accounted for the nonlinear behavior of the DER model. Furthermore, their approach relies on a linear model predictive controller, while MGs exhibit nonlinear characteristics.

To overcome these challenges, our research introduces a centralized NLMPC approach tailored for microgrid systems. NLMPC excels in handling continuous control variables, vital for real-time power sharing and load balancing in microgrids

This work was in part under support from the National Science Foundation under Grant NSF-EPCN 2221784 and the Department of Defense, Office of Naval Research award number N00014-23-1-2602 and was financed (in part) by a grant from the Commonwealth of Pennsylvania, Department of Community and Economic Development, through the Pennsylvania Infrastructure Technology Alliance (PITA). The authors are with the Department of Electrical and Computer Engineering, Lehigh University, Bethlehem, PA, USA (e-mails: masb22@lehigh.edu, khazaei@lehigh.edu,moazeni@lehigh.edu).

Authorized licensed use limited to: LEHIGH UNIVERSITY. Downloaded on June 09,2024 at 16:25:19 UTC from IEEE Xplore. Restrictions apply.
© 2024 IEEE. Personal use is permitted, but republication/redistribution requires IEEE permission. See https://www.ieee.org/publications/rights/index.html for more information.

This article has been accepted for publication in IEEE Transactions on Energy Conversion. This is the author's version which has not been fully edited and content may change prior to final publication. Citation information: DOI 10.1109/TEC.2024.3365353

Table I. Comparison between the controllers for MG energy management.

Characteristics/ Controller	Ref.	Nonlinear model handling	Constraints handling	Optimal control handling	Dispatchability	P, and Q load and demand satisfying	MIMO system handling	Real-time implementation
PI	[3]	×	×	×	×	×	×	✓
NN-based	[4], [5]	✓	×	×	✓	✓	✓	✓
NLMPC	Proposed	✓	✓	✓	✓	✓	✓	✓

Table II. Comparison between the state-Of-the-art model identification method.

Ref.	Method	Non-linear Model Identification	Closed-form Solution	Grey-box
[12], [13]	Hammesterian	×	×	✓
[14], [15]	NN	✓	×	✓
[16]	Iterative Least-square	✓	✓	×
[17]	Physics-informed NN	✓	×	×
[18], [19], [20]	DMD	×	×	×
Proposed	SR	✓	✓	✓

in contrast to the discrete (integer) control sets of finite control set MPC (FCS-MPC) [21], aligns better with the dynamic requirements of our microgrid, facilitating effective and flexible management of power distribution and load balance.

Nonlinear controllers, such as NLMPC have emerged as effective solutions for managing MGs, offering predictable performance across a wide range of operating conditions. As an example, real-time implementation of rapid secondary control utilizing NLMPC was proposed in [22]. Nonetheless, the proposed approach only considered conventional MG structure with simplified dynamics of synchronous generators and did not account for DERs and their dynamics. In addition, the heavy reliance of conventional NLMPC techniques on accurate dynamic models of assets make it very challenging for real-time control of MGs that have various assets with different topologies and dynamic models. Hence, the absence of accurate models poses significant obstacles for employing NLMPC-based control in MGs that incorporate DERs for the purpose of power sharing. The main research question in this paper is "can data-driven modeling techniques resolve the modeling challenge of NLMPC approaches for MG control?"

Recent machine learning advancements have introduced diverse methodologies for modeling dynamic systems, as detailed in a comprehensive comparison in Table II. These include Hammesterian, neural networks (NN), physics-informed neural networks, Iterative least-square, dynamic mode decomposition (DMD), and SR [23]. Each method varies in its ability to identify non-linear models, provide closed-form solutions, and the extent of prior knowledge dependency. For instance, the Hammerstein model [12], [13], lacks in non-linear identification and closed-form solution, yet offers grey-box insights, while NN methods ([14], [15],[17]) excel in non-linear identification but fall short in providing closed-form solutions, with varying degrees of transparency in their modeling process. Among these, SR stands out for its proficiency in non-linear model identification, offering closed-form solutions within a grey-box framework, marking a significant methodological advancement. In contrast, DMD ([18], [19], [20]) primarily supports linear dynamics and lacks both a closed-form solution and grey-box classification. The Iterative Least-square method [16] strikes a balance with its non-linear model identification and closed-form solution, though it doesn't qualify as a grey-box model. Additionally, SR's capability to work with limited data, its fast convergence, reduced training time, and interpretability positions it as a favorable option compared to other model identification methods [23]. As a result, the main contribution of this paper is to develop a data-driven NLMPC framework for MGs using SR theory. To the best of our knowledge, no existing studies have explored a data-driven NLMPC for MG control that can solve the heavy reliance of MG MPC techniques on accurate physics-based models.

In this paper, we address the limitation of previous studies by developing a data-driven NLMPC approach for MG control. Specifically, the paper enumerates its distinguished contributions as follows:

1) This paper presents a novel model identification method for both nonlinear and linear DERs in smart grids. Compared with deep learning approaches, the proposed method utilizes available DER measurements and eliminates the need for extensive training.
2) By employing a data-driven framework, we simplify the complex physics-based DER modeling approach commonly used, while still providing a scalable framework for DER control. This framework effectively addresses power sharing issues observed in conventional DER control.
3) Obtained data-driven DER models in this study will be utilized to develop a comprehensive framework for MG's NLMPC control. This framework enables simultaneous control of the primary and secondary layers of the MG. By integrating both layers into a single framework, the control capabilities of the MG are enhanced and the control design is simplified (compared with conventional hierarchical controllers).
4) The robustness of the proposed data-driven NLMPC is demonstrated, exhibiting superior performance in comparison to a MPC controller that utilizes successive linearization.
5) The experimental applicability of the proposed data-driven NLMPC control has been validated using OPAL-RT real-time simulation technologies, confirming its effectiveness and reliability for real-world, real-time operations.

The paper is outlined as follows: Section II covers the proposed methodology with MG modeling. Section III focuses on the data-driven modeling of the MG consist of DERs and diesel generator using SR. Design of data-driven controller is discussed in Section IV. Section V includes the case studies, and finally, section VI concludes the paper.

Authorized licensed use limited to: LEHIGH UNIVERSITY. Downloaded on June 09,2024 at 16:25:19 UTC from IEEE Xplore. Restrictions apply.
© 2024 IEEE. Personal use is permitted, but republication/redistribution requires IEEE permission. See https://www.ieee.org/publications/rights/index.html for more information.

This article has been accepted for publication in IEEE Transactions on Energy Conversion. This is the author's version which has not been fully edited and content may change prior to final publication. Citation information: DOI 10.1109/TEC.2024.3365353

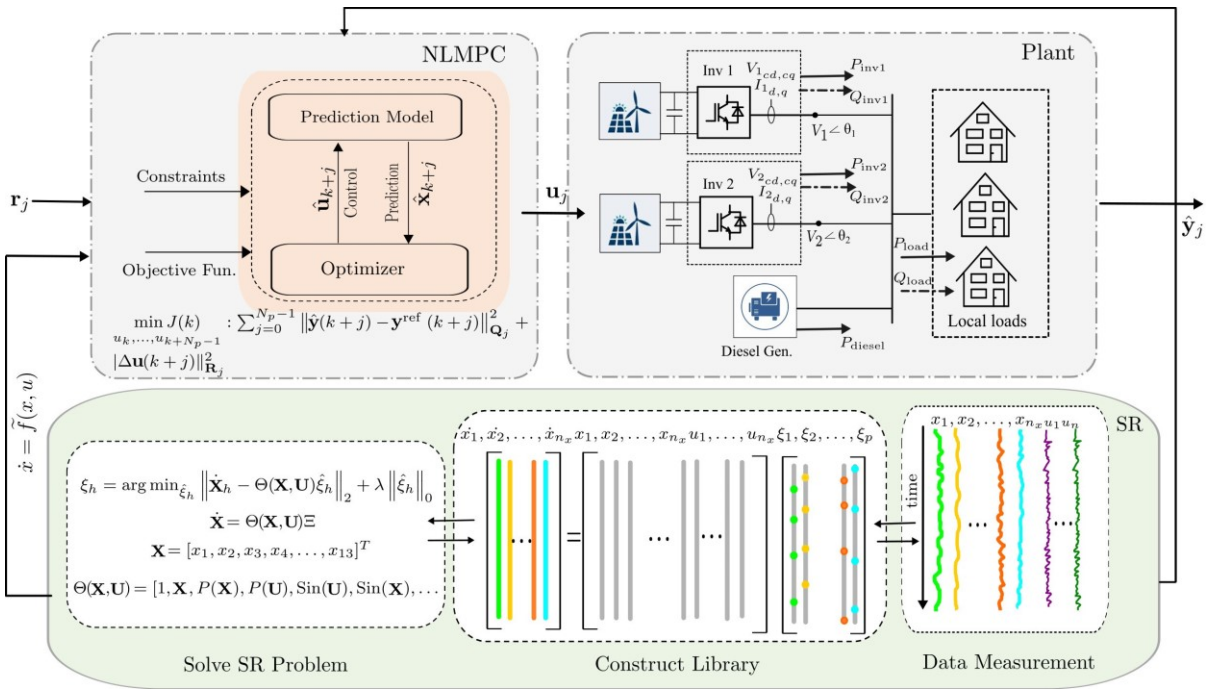

Fig. 1. The proposed schematic of SRc-based NLMPC framework for active and reactive power sharing.

II. Methodology

A. Proposed Model Description

Fig. 1 presents an illustrative depiction of the proposed methodology for data-driven model identification utilizing SR in conjunction with NLMPC. We opted for NLMPC over other MPC approaches including distributed MPC or finite control MPC due to the fact that microgrids are controlled centrally as well as suitability of NLMPC in a centralized control context, particularly for managing the three main resources of our microgrid system. The system under consideration closely resembles an islanded MG and comprises two inverter-based resources, one diesel generator, and local loads.

Initially, the SR technique is employed to identify the dynamic model of the solely through measured data. Subsequently, the identified dynamics which can be represented by $\hat{\boldsymbol{x}}(k+1) = \tilde{\boldsymbol{f}}(\hat{\boldsymbol{x}}, \boldsymbol{u})$ are integrated within the NLMPC framework, thereby facilitating the formulation of a data-driven optimal control problem with power sharing and load balancing features embedded as constraints of the optimization. The control inputs obtained from the NLMPC formulation, denoted as $\boldsymbol{u_j}$, are sent to the MG in close to real-time for dispatching the assets. In the following sections, physics-based modeling of MG will be included as a ground truth for data-driven methods.

B. Microgrid Modeling

1) Modeling of the Inverter-based resources: For the inverter-based resource model, a voltage source inverter with droop control is considered (see Fig. 2). The DER's effective terminal voltage and phase angle after passing through the LC filters are represented as $V \angle \theta$. Our chosen 5th-order reduced-order model in the dq frame is based on a balance between computational efficiency and the ability to accurately capture the inverter's detailed dynamics. This model is validated against more detailed models, as explored in [24] ensuring its reliability for stability assessment in MGs. The model is described by the following set of equations:

$$\dot{\theta} = \omega(t) - \omega_0 \tag{1a}$$

$$\tau\dot{\omega} = \omega_{set}(t) - \omega(t) - \frac{k_p\omega_0}{S_n} P_m(t) \tag{1b}$$

$$\tau\dot{V} = V_{set}(t) - V(t) - \frac{k_q}{S_n} Q_m(t) \tag{1c}$$

$$L\dot{I}_d = V(t)\cos\theta(t) - V_0 - RI_d(t) + \omega_0 LI_q(t) \tag{1d}$$

$$L\dot{I}_q = V(t)\sin\theta(t) - RI_q(t) - \omega_0 LI_d(t) \tag{1e}$$

where $V(t)$ in V and $\theta(t)$ in radians, represent the instantaneous effective terminal voltage and phase angle of the DER, respectively. Also, $\omega(t)$ in radian/s denotes the frequency of the DER and $I_d(t)$ and $I_q(t)$ in A represent the dq-frame components of the DER's output current. The model also incorporates the low-pass filters in the inverter power control system, which is characterized by the bandwidth $w_c = \tau^{-1}$, and k_p and k_q are the frequency and voltage droop gains, respectively. The parameters of the this DER are further shown in Table VI.

Furthermore, S_n represents the DER rating, while $\omega_{set}(t)$ and $V_{set}(t)$ are the set points of frequency and voltage controllers considered as inputs of the DER. Measured instantaneous active and reactive powers, $P_m(t)$ and $Q_m(t)$, are given by $P_m(t) = \frac{3}{2}V(t)I_d(t)$ and $Q_m(t) = -\frac{3}{2}V(t)I_q(t)$. Finally, $L = L_c + L_l$ in mH and $R = R_c + R_l$ in mΩ represent the combined inductance and resistance at the DER terminal.

2) Modeling of the Diesel Generator: In this study, the generator model is represented by its load frequency control (LFC) loop, focusing on its contributions to the active power

Authorized licensed use limited to: LEHIGH UNIVERSITY. Downloaded on June 09,2024 at 16:25:19 UTC from IEEE Xplore. Restrictions apply.
© 2024 IEEE. Personal use is permitted, but republication/redistribution requires IEEE permission. See https://www.ieee.org/publications/rights/index.html for more information.

This article has been accepted for publication in IEEE Transactions on Energy Conversion. This is the author's version which has not been fully edited and content may change prior to final publication. Citation information: DOI 10.1109/TEC.2024.3365353

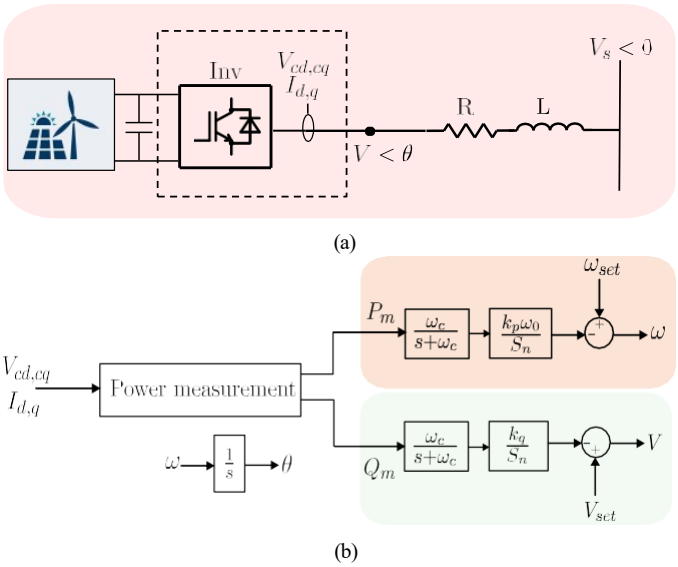

Fig. 2. Overview of inverter-based resource control system: (a) displays the configuration of the DER with an inverter, and (b) details the droop control mechanism.

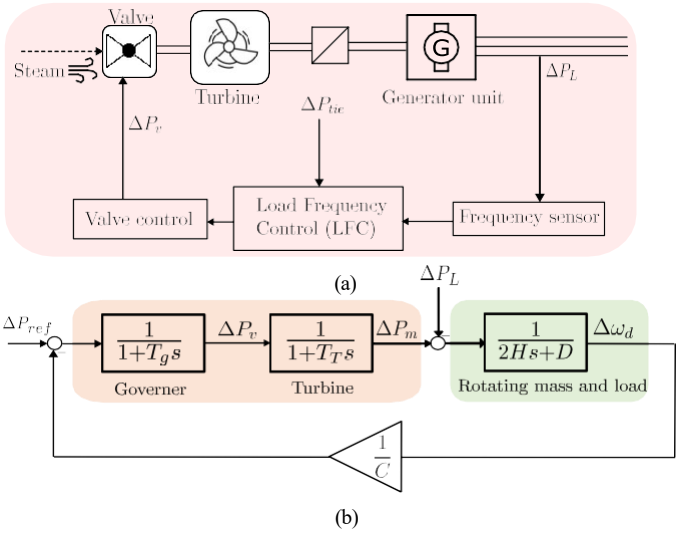

Fig. 3. Schematic overview of diesel generator load frequency control: (a) presents the block diagram of the automatic load frequency control system, and (b) illustrates the detailed control loop components for the diesel generator.

and frequency regulation in islanded MGs. Fig. 3 shows the LFC loop composed of a governor, prime mover load, and rotating mass model presented in state-space form as [25]:

$$\Delta\dot{P}_v = -\frac{1}{T_g}\Delta P_v(t) - \frac{1}{RT_g}\Delta\omega_d(t) + \frac{1}{T_g}\Delta P_{ref}(t) \quad (2a)$$

$$\Delta\dot{P}_m = \frac{1}{T_T}\Delta P_v(t) - \frac{1}{T_T}\Delta P_m(t) \quad (2b)$$

$$\Delta\dot{\omega}_d = \frac{1}{2H}\Delta P_m(t) - \frac{D}{2H}\Delta\omega_d(t) - \frac{1}{2H}\Delta P_L(t) \quad (2c)$$

where $[\Delta P_v(t)\ \Delta P_m(t)\ \Delta\omega_d(t)]^T$ are states of the diesel generator and $\Delta P_L(t)$ is the input of the system with $\Delta P_{ref}(t) = 0$ [25]. In the above equations, the input governor's command ΔP_g is converted into a steam valve position ΔP_v, the governor time constant T_g in seconds characterizes the response time of the governor, and the T_T in seconds represents turbine time constant. The prime mover model, denoted as ΔP_m, establishes a relationship between the mechanical power output and variations in the steam valve position ΔP_v.

C. Control Oriented Model

It was shown that each DER is characterized by 5 dynamical equations, while the diesel generator contributes 3 dynamical equations. Consequently, the overall plant of the system encompasses a total of 13 dynamical equations formulated as:

$$\begin{aligned} \dot{\boldsymbol{x}} &= \boldsymbol{f}(\boldsymbol{x}) + \boldsymbol{g}(\boldsymbol{u}) + \boldsymbol{d} \\ \boldsymbol{y} &= \boldsymbol{h}(\boldsymbol{x}) \end{aligned} \quad (3)$$

where

$$\begin{aligned} \boldsymbol{x} &= [\theta_1\ \omega_1\ V_1\ I_{d1}\ I_{q1}\ \theta_2\ \omega_2\ V_2\ I_{d2}\ I_{q2}\ \Delta P_v\ \Delta P_m\ \Delta\omega_d]^T \\ \boldsymbol{u} &= [\omega_{set1}\ V_{set1}\ \omega_{set2}\ V_{set2}\ \Delta P_L]^T \\ \boldsymbol{d} &= [\omega_0\ 0\ 0\ V_0\ 0\ \omega_0\ 0\ 0\ V_0\ 0\ 0\ 0\ 0]^T \end{aligned} \quad (4)$$

and $\mathbf{f}(\mathrm{x})$ defined on the top of the page and $\mathbf{g}(\mathrm{u})$ is defined as

$$\mathbf{g}(\mathrm{u}) = \begin{bmatrix} 0 & 0 & 0 & 0 & 0 \\ \frac{1}{t_1} & 0 & 0 & 0 & 0 \\ 0 & \frac{1}{t_1} & 0 & 0 & 0 \\ 0 & 0 & 0 & 0 & 0 \\ 0 & 0 & 0 & 0 & 0 \\ 0 & 0 & \frac{1}{t_2} & 0 & 0 \\ 0 & 0 & 0 & \frac{1}{t_2} & 0 \\ 0 & 0 & 0 & 0 & 0 \\ 0 & 0 & 0 & 0 & 0 \\ 0 & 0 & 0 & 0 & \Delta P_L \end{bmatrix} \quad (5)$$

To achieve efficient power sharing, it is crucial to satisfy the load balance constraint, which can be expressed as

$$\begin{aligned} P_{load}(t) &= P_{inv1}(t) + P_{inv2}(t) + P_{diesel}(t) \\ Q_{load}(t) &= Q_{inv1}(t) + Q_{inv2}(t) \end{aligned} \quad (6)$$

In the given context, the variables $P_{load}(t)$ and $Q_{load}(t)$ represent the active and reactive power of the load, respectively. The active power measurements of DERs are given by $P_{inv1}(t) = \frac{3}{2}V_1(t)I_{d1}(t)$ and $P_{inv2}(t) = \frac{3}{2}V_2(t)I_{d2}(t)$. The diesel generator's measured active power is represented by $\Delta P_m(t)$. Similarly, the reactive power of DER1 and DER2 are $Q_{inv1}(t) = -\frac{3}{2}V_1(t)I_{q1}(t)$ and $Q_{inv2}(t) = -\frac{3}{2}V_2(t)I_{q2}(t)$, respectively. Equation (6) can be reformulated as $P_{load} = \frac{3}{2}x_3x_4 + \frac{3}{2}x_8x_9 + x_{12}$ and $Q_{load} = -\frac{3}{2}x_3x_5 + -\frac{3}{2}x_9x_{10}$, which can be presented as $\boldsymbol{y} = \boldsymbol{h}(\boldsymbol{x})$ of the problem [26].

In order to ensure the feasibility of the system operation, the generation capacities of the MG components must be taken into account as constraints. The active power constraints are outlined as:

$$\begin{aligned} P_{inv1,min} \le P_{inv1}(t) \le P_{inv1,max} \\ P_{inv2,min} \le P_{inv2}(t) \le P_{inv2,max} \\ P_{diesel,min} \le P_{diesel}(t) \le P_{diesel,max} \end{aligned} \quad (7)$$

Authorized licensed use limited to: LEHIGH UNIVERSITY. Downloaded on June 09,2024 at 16:25:19 UTC from IEEE Xplore. Restrictions apply.
© 2024 IEEE. Personal use is permitted, but republication/redistribution requires IEEE permission. See https://www.ieee.org/publications/rights/index.html for more information.

This article has been accepted for publication in IEEE Transactions on Energy Conversion. This is the author's version which has not been fully edited and content may change prior to final publication. Citation information: DOI 10.1109/TEC.2024.3365353

$$\mathbf{f}(\mathrm{x}) = \begin{bmatrix} \mathrm{x}_2, \\ -\frac{1}{L_1}\mathrm{x}_3\cos(\mathrm{x}_1) + \frac{R_1}{L_1}\mathrm{x}_4 + \omega_0\mathrm{x}_5, \\ -\frac{1}{\tau_2}\mathrm{x}_7 + \frac{k_{p_2}\omega_0}{S_n\tau_2}\mathrm{x}_8\mathrm{x}_9, \\ -\frac{1}{L_2}\mathrm{x}_8\sin(\mathrm{x}_6) + \frac{R_2}{L_2}\mathrm{x}_{10} + \omega_0\mathrm{x}_9, \\ \frac{1}{2H}\mathrm{x}_{12} - \frac{D}{2H}\mathrm{x}_{13} \end{bmatrix} \begin{bmatrix} -\frac{1}{\tau_1}\mathrm{x}_2 + \frac{k_{p_1}\omega_0}{S_n\tau_1}\mathrm{x}_3\mathrm{x}_4, \\ -\frac{1}{L_1}\mathrm{x}_3\sin(\mathrm{x}_1) + \frac{R_1}{L_1}\mathrm{x}_5 + \omega_0\mathrm{x}_4, \\ -\frac{1}{\tau_2}\mathrm{x}_8 + \frac{k_{q_2}}{S_n\tau_2}\mathrm{x}_8\mathrm{x}_{10}, \\ -\frac{1}{T_g}\mathrm{x}_{11} - \frac{1}{CT_g}\mathrm{x}_{13}, \end{bmatrix} \begin{bmatrix} -\frac{1}{\tau_1}\mathrm{x}_3 + \frac{k_{q_1}}{S_n\tau_1}\mathrm{x}_3\mathrm{x}_5, \\ \mathrm{x}_7, \\ -\frac{1}{L_2}\mathrm{x}_8\cos(\mathrm{x}_6) + \frac{R_2}{L_2}\mathrm{x}_9 + \omega_0\mathrm{x}_{10}, \\ \frac{1}{T_T}\mathrm{x}_{11} - \frac{1}{T_T}\mathrm{x}_{12}, \end{bmatrix}^T$$

Similarly, the reactive power constraints can be expressed as:

$$\begin{aligned} \mathrm{Q}_{\mathrm{inv1,min}} \le \mathrm{Q}_{\mathrm{inv1}}(\mathrm{t}) \le \mathrm{Q}_{\mathrm{inv1,max}} \\ \mathrm{Q}_{\mathrm{inv2,min}} \le \mathrm{Q}_{\mathrm{inv2}}(\mathrm{t}) \le \mathrm{Q}_{\mathrm{inv2,max}} \end{aligned} \tag{8}$$

To ensure microgrid stability, it is essential to set appropriate active (K_p) and reactive (K_q) droop gains to maintain energy resources within specified voltage and frequency bounds. These bounds are defined such that voltage and frequency should remain within ±5% of their nominal values [27], represented by ΔV and $\Delta\omega$, respectively. The droop gains are calculated using the formulae $K_p = \frac{\Delta\omega}{\Delta P}$ and $K_q = \frac{\Delta V}{\Delta Q}$. Here, ΔP and ΔQ denote the capacity limits of the DERs in active and reactive power, respectively. These capacities are critical in ensuring that the DERs can effectively manage their output within these stability constraints.

Additionally, power distribution allocations are directly influenced by these calculated droop gains. The allocations are based on preliminary assessments and are represented by equations $\alpha P_{\mathrm{inv2}}(t) = P_{\mathrm{inv1}}(t)$, $\beta P_{\mathrm{diesel}}(t) = P_{\mathrm{inv1}}(t)$, and $\gamma Q_{\mathrm{inv2}}(t) = Q_{\mathrm{inv1}}(t)$. The coefficients α, β, and γ were determined through these assessments to ensure optimal power sharing among different generation sources. This takes into account their capacity, efficiency, and response characteristics to maintain system stability under varying load conditions. The values of α, β, and γ have been set as 1.1, 5.8, and 1.08, respectively, to achieve this balance.

III. SR FOR IDENTIFYING MICROGRID DYNAMICS

In this section, we apply the SR algorithm as a data-driven model identification step within the proposed NLMPC framework. The process of determining the governing equations from measured data involves three distinct steps, which are outlined in the following.

A. Preparing Data for Identifying the Governing Equations

Most dynamical systems are represented by differential equations in the form $\boldsymbol{x}^{\cdot} = \boldsymbol{f}(\boldsymbol{x}, \boldsymbol{u})$. These systems typically have a relatively small number of terms on the right-hand side. To prepare data for measurement, we introduce small perturbations to the input data—specifically, applying sine waves that do not exceed 10% of the nominal values (as detailed in [28]), This approach facilitates the acquisition of m measurement samples, encompassing states, derivatives, and inputs from the DERs and diesel generator. Consequently, the dynamics of the MG can be deduced. This is achieved by employing a library of potential functions, denoted as $\boldsymbol{\Theta} \in \mathbb{R}^{m\times p}$, where p is the count of functions within the library [23]. In most practical systems, access is typically limited to $\boldsymbol{x}(t)$ and $\boldsymbol{u}(t)$, necessitating the numerical approximation of the derivative measurements $\boldsymbol{x}^{\cdot}(t)$. The process begins with sampling the measurement data at intervals $t_1, t_2, \ldots, t_m$, which are then systematically organized into a matrix, as follows:

$$\boldsymbol{X} = \begin{bmatrix} \mathrm{x}_1(t_1) & \mathrm{x}_2(t_1) & \ldots & \mathrm{x}_{n_x}(t_1) \\ \mathrm{x}_1(t_2) & \mathrm{x}_2(t_2) & \ldots & \mathrm{x}_{n_x}(t_2) \\ \vdots & \vdots & \ddots & \vdots \\ \mathrm{x}_1(t_m) & \mathrm{x}_2(t_m) & \ldots & \mathrm{x}_{n_x}(t_m) \end{bmatrix} \tag{9}$$

$$\boldsymbol{U} = \begin{bmatrix} \mathrm{u}_1(t_1) & \mathrm{u}_2(t_1) & \ldots & \mathrm{u}_{n_u}(t_1) \\ \mathrm{u}_1(t_2) & \mathrm{u}_2(t_2) & \ldots & \mathrm{u}_{n_u}(t_2) \\ \vdots & \vdots & \ddots & \vdots \\ \mathrm{u}_1(t_m) & \mathrm{u}_2(t_m) & \ldots & \mathrm{u}_{n_u}(t_m) \end{bmatrix} \tag{10}$$

To identify the dynamics from data $(\boldsymbol{X}, \boldsymbol{U})$, $\dot{\boldsymbol{X}}$ is also needed. In this work, the central difference approximation is adopted due to its superior accuracy when dealing with smooth functions [23]. Accordingly, the derivative matrix $\mathrm{X}^{\cdot}$ is approximated as:

$$\dot{\boldsymbol{X}} \approx \frac{\boldsymbol{X}(\mathrm{j}+1) - \boldsymbol{X}(\mathrm{j}-1)}{2s_p} \tag{11}$$

Here, $\boldsymbol{X}(\mathrm{j}+1)$ denotes the measured data at sample $\mathrm{j}+1$, and s_p represents the sampling time of the simulation or data collection platform.

B. Establishing Candidate Nonlinear Functions

In this step, a collection of candidate functions $(\boldsymbol{\Theta}(\boldsymbol{X}, \boldsymbol{U}))$ can be assembled to effectively capture the temporal variations of the state variables. In situations where prior knowledge of the system's dynamics is lacking, it becomes necessary to select an expanded set of candidate functions that encompasses all potential functions. It is notable that, in the context of MGs, the function $\boldsymbol{f}(\boldsymbol{x}, \boldsymbol{u})$ exhibits sparsity in the space of all potential candidate functions, as only a limited number of nonlinear terms are present, such as $V\sin\theta$, and $V\cos\theta$ [29]. The derivative data of the states , obtained using the measured data $\boldsymbol{X} \in \mathbb{R}^{m\times n_x}$, can be expressed as a linear combination of columns from a candidate function library, such as polynomials or sinusoids using the entries of the matrix $\boldsymbol{\Xi} \in \mathbb{R}^{p\times n_x}$ in equation (12):

$$\boldsymbol{X}^{\cdot} = \boldsymbol{\Theta}(\boldsymbol{X}, \boldsymbol{U})\boldsymbol{\Xi}. \tag{12}$$

Typical candidate functions include monomials and trigonometric functionspresented in equation (13):

Authorized licensed use limited to: LEHIGH UNIVERSITY. Downloaded on June 09,2024 at 16:25:19 UTC from IEEE Xplore. Restrictions apply.
© 2024 IEEE. Personal use is permitted, but republication/redistribution requires IEEE permission. See https://www.ieee.org/publications/rights/index.html for more information.

This article has been accepted for publication in IEEE Transactions on Energy Conversion. This is the author's version which has not been fully edited and content may change prior to final publication. Citation information: DOI 10.1109/TEC.2024.3365353

$$\boldsymbol{\Theta}^T(\boldsymbol{X},\boldsymbol{U}) = \begin{bmatrix} 1 \\ \boldsymbol{X} \\ \boldsymbol{X}^2 \\ \boldsymbol{U} \\ \vdots \\ \sin(\boldsymbol{X},\boldsymbol{U}) \\ \cos(\boldsymbol{X},\boldsymbol{U}) \\ \boldsymbol{X}\sin(\boldsymbol{X},\boldsymbol{U}) \\ \vdots \end{bmatrix} \quad (13)$$

C. SR Algorithm

After estimating $\dot{\boldsymbol{X}}$ and determining $\boldsymbol{\Theta}(\boldsymbol{X}, \boldsymbol{U})$ using the available $\boldsymbol{X}$ and $\boldsymbol{U}$ data, data-driven dynamics $\dot{\boldsymbol{X}} = \boldsymbol{\Theta}(\boldsymbol{X}, \boldsymbol{U})\boldsymbol{\Xi}$ can be obtained by solving for the sparse matrix of coefficients in $\boldsymbol{\Xi}$. This matrix represents the active terms in the dynamics of $\dot{\boldsymbol{X}}$, which is accomplished by solving an optimization problem as shown in equation (14).

$$\xi_i = \arg\min_{\hat{\xi}_i} \frac{1}{2}\|\dot{\boldsymbol{X}}_i - \boldsymbol{\Theta}(\boldsymbol{X},\boldsymbol{U})\hat{\xi}_i\|_2 + \eta\|\hat{\xi}_i\|_0 \quad (14)$$

where, ξ_i represents the i-th column of Ξ denoted by $\boldsymbol{\Xi}_i = \begin{bmatrix} \xi_1 & \xi_2 & \dots & \xi_p \end{bmatrix}^T$. The term $\dot{\boldsymbol{X}}_i$ corresponds to the i-th column of $\dot{\boldsymbol{X}}$. The objective function in equation (14) minimizes the error between the actual derivatives $\dot{\boldsymbol{X}}$ and the estimated derivatives obtained through a least-squares problem using the calculated ξ_i. The minimization is performed using the L2 norm $\|\cdot\|_2$. Furthermore, the L0 norm $\|\cdot\|_0$ is employed to minimize the number of nonzero elements in ξ_i, promoting sparsity in the coefficient matrix Ξ. The regularization parameter η plays a crucial role in controlling the degree of sparsity in the solution and can be fine-tuned through hyper-parameter tuning techniques [30].

Algorithm 1: SR-Based Model Identification

Data: $\boldsymbol{X}, \boldsymbol{U}$ (Measurements)
Data: $\dot{\boldsymbol{X}}$ (Estimated derivatives)
Result: Sparse matrix $\boldsymbol{\Xi}$
Compute the coefficient matrix: $\boldsymbol{\Xi} = \boldsymbol{\Theta} \setminus \dot{\boldsymbol{X}}$ **for** $\varepsilon = 1 : T$ **do**
  Set the sparsity parameter: η Find indices of small coefficients: $\text{ind}_{small} = |\Xi| < \eta$;
  Set small coefficients to zero: $\Xi(\text{ind}_{small}) \leftarrow 0$;
  for $\varepsilon = 1 : n_x$ **do**
    Find indices of remaining coefficients: $\text{ind}_{big} = \text{ind}_{small}(:, \varepsilon)$;
    Update remaining coefficients: $\Xi(\text{ind}_{big}, \varepsilon) = \Theta(:, \text{ind}_{big}) \setminus \dot{X}(:, \varepsilon)$;
  end
end

IV. Data-driven Control Design

Fig. 4 provides an illustrative representation of MPC approach. The prediction model is constructed by incorporating the controlled system model and the present state values. Subsequently, an optimization algorithm is employed to generate an optimal sequence of control actions over a prediction horizon [31]. In this study, in order to control the model obtained through the SR technique, NLMPC will be employed to regulate and control the MG assets. The objective of utilizing NLMPC is to achieve power balance while ensuring that voltage and frequency remain within permissible limits.

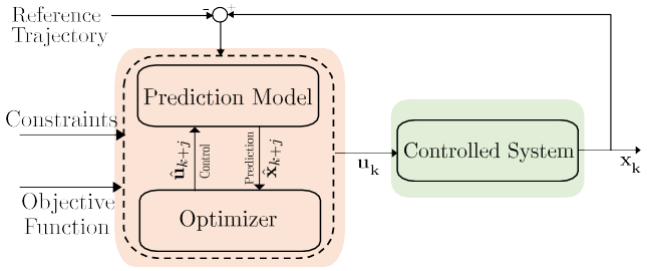

Fig. 4. Schematic diagram of the MPC controller.

A. SR with optimal control problem formulation (SRc)

MPC minimizes a tracking error, aligning system states with desired set-points, while also reducing controller rate of change for increased longevity [32]. To achieve these objectives, the system's dynamics, obtained using the SR method, can be represented by $\dot{\hat{\boldsymbol{x}}} = \boldsymbol{\Theta}(\hat{\boldsymbol{x}}, \boldsymbol{u})\boldsymbol{\Xi}$ and discretized for implementation in the MPC framework expressed by $\hat{\boldsymbol{x}}(k+1) = \tilde{\mathbf{f}}(\hat{\boldsymbol{x}}, \boldsymbol{u})$. By integrating the MG's data-driven dynamics described as $\hat{\boldsymbol{x}}(k+1) = \tilde{\mathbf{f}}(\hat{\boldsymbol{x}}, \boldsymbol{u})$ with the inclusion of physical and droop constraints imposed on the states, the ultimate formulation of the NLMPC is presented as follows:

$$\min_{u_k,\dots,u_{k+N_p-1}} J(k) := \quad (15)$$

$$\sum_{j=0}^{N_p-1} \|\hat{\boldsymbol{y}}(k+j) - \boldsymbol{y}^{ref}(k+j)\|^2_{\boldsymbol{Q}_j} + \|\Delta\boldsymbol{u}(k+j)\|^2_{\boldsymbol{R}_j}$$

$$\text{s.t.} \quad \hat{\boldsymbol{x}}(k+j+1) = \tilde{\boldsymbol{f}}(\hat{\boldsymbol{x}}(k+j), \boldsymbol{u}(k+j)), \quad (16)$$

$$j = 0, 1, \dots, N_p - 1$$

$$\underline{u} \le \boldsymbol{u}(k+j) \le \bar{u}, \quad j = 0, 1, \dots, N_p - 1 \quad (17)$$

$$\underline{y} \le \hat{\boldsymbol{y}}(k+j) \le \bar{y}, \quad j = 1, 2, \dots, N_p \quad (18)$$

$$\hat{\boldsymbol{x}}_0 = \boldsymbol{x}_{plant}(k_0) \quad (19)$$

where, the notation $N_p \in \mathbb{N}^+$ represents the prediction horizon, while $k := kt_s \in \mathbb{R}^+$ denotes the current time step based on the sampling time t_s. The penalty weights for the states and control inputs are denoted by $\boldsymbol{Q} \succ 0$ and $\boldsymbol{R} \succ 0$ respectively. The variables $\hat{\boldsymbol{x}}(k) \in \mathbb{R}^{n_x}$, $\boldsymbol{u}(k) \in \mathbb{R}^{n_u}$, and $\Delta\boldsymbol{u}(k) \in \mathbb{R}^{n_u}$ represent the states, input, and rate of change of input at time step k respectively. The desired set-points are represented by $y^{ref} \in \mathbb{R}^{n_x}$ which is the function of $\hat{\boldsymbol{x}}(k)$. Furthermore, $\underline{x}$, $\underline{u}$, $\bar{x}$, and $\bar{u}$ correspond to the minimum and maximum values for the states and control inputs respectively. Lastly, the function $\tilde{\boldsymbol{f}} : \mathbb{R}^{n_x+n_u} \to \mathbb{R}^{n_x}$ denotes the discretized prediction model, which exhibits varying formulations and is further elucidated in the next subsection.

Authorized licensed use limited to: LEHIGH UNIVERSITY. Downloaded on June 09,2024 at 16:25:19 UTC from IEEE Xplore. Restrictions apply.
© 2024 IEEE. Personal use is permitted, but republication/redistribution requires IEEE permission. See https://www.ieee.org/publications/rights/index.html for more information.

This article has been accepted for publication in IEEE Transactions on Energy Conversion. This is the author's version which has not been fully edited and content may change prior to final publication. Citation information: DOI 10.1109/TEC.2024.3365353

1) Nonlinear MPC: NLMPC relies on a direct utilization of the discretized nonlinear dynamics of the system $\boldsymbol{x}(k+1) = \tilde{\mathbf{f}}(\boldsymbol{x}(k), \boldsymbol{u}(k))$. Consequently, the prediction model over next N_p prediction horizons can be written as (16). The algorithm for the implementation of the proposed SR-based NLMPC for MG control in this study can be found in algorithm 2. To

Algorithm 2: SR-based NLMPC (SRc)

Data: $N_p, \mathbf{Q}, \mathbf{R}, T, n_x, n_u, \boldsymbol{x}^{ref}, \mathbf{f}(\boldsymbol{x}, \boldsymbol{u})$
Initialize $\boldsymbol{x}_0 \in \mathbb{R}^{nx}, \boldsymbol{u}_0 \in \mathbb{R}^{nu}, k = 0$; **for** $k = 0$ *to* $T - 1$ **do**
  ▷ Simulation time
  for $j = 0$ *to* $N_p - 1$ **do**
    Define and discretize the state space model;
    Construct the data-driven model; Formulate the quadratic cost function: $J(\boldsymbol{x}(k+j), \boldsymbol{u}(k+j))$, in equation (15);
  end
  Solve the optimization problem by minimizing $J(k)$ subject to the dynamic and state constraints defined in Eqs. (16)–(18);
  Extract the optimal control sequence $[\boldsymbol{u}^*(0|k), \ldots, \boldsymbol{u}^*(N_p - 1|k)]$;
  Apply only the first control action $\boldsymbol{u}^*(0|k)$;
  Predict the next state $\boldsymbol{x}(k+1|k)$ using equation (16);
  Update the initial conditions for the next iteration: $\boldsymbol{x}_0 = \boldsymbol{x}(k+1|k)$ and $\boldsymbol{u}_0 = \boldsymbol{u}^*(0|k)$;
end

solve this NLMPC problem in equations (15) to (19), sequential quadratic programming (SQP) was utilized. SQP is an iterative technique widely employed for solving nonlinear constrained optimization problems by sequentially solving a series of quadratic programming (QP) sub-problems, as described in equation (21) [33]. The SQP algorithm initiates with an initial estimate $\boldsymbol{x}^k$ for a given iteration index k, and it advances through iterative updates given by $\boldsymbol{x}^{k+1} := \boldsymbol{x}^k + \alpha \boldsymbol{p}_k$, where $\boldsymbol{p}_k$ denotes the search direction. The updated estimate $\boldsymbol{x}^{k+1}$ is subsequently utilized to solve the QP sub-problem, yielding $\boldsymbol{p}$ as the solution. This iterative process generates a sequence of $\boldsymbol{x}^k$ values, aiming to converge towards a local minimum x^* as the iteration count k approaches infinity.

The decision variables ($\boldsymbol{x}^k$) for the formulated nonlinear optimization problem encompass the rate of change of the control input ($\Delta \boldsymbol{U} \in \mathbb{R}^{n_u N_p}$) and the states ($\boldsymbol{X} \in \mathbb{R}^{n_x N_p}$). The Lagrangian function associated with the nonlinear problem presented in equations (15)-(19) is defined as[33]:

$$\mathsf{L}(x, \lambda, \mu) := \mathrm{f}(\boldsymbol{x}) + \sum_{i=1}^{m} \lambda_i \boldsymbol{h}_i(x) + \sum_{i=1}^{p} \mu_j \boldsymbol{g}_j(x) \qquad (20)$$

where the functions $h : \mathbb{R}^n \to \mathbb{R}^m$ and $g : \mathbb{R}^n \to \mathbb{R}^p$ represent the equality and inequality constraints, respectively, derived from the concatenation of (16)-(18). Furthermore, n, m, and p denote the number of decision variables, equality constraints, and inequality constraints, respectively. The Lagrangian multipliers for the associated equality and inequality constraints are denoted as $\lambda \in \mathbb{R}^m$ and $\mu \in \mathbb{R}^n$, respectively.

The formulation of the QP subproblem involves the approximation of the Lagrangian function given in equation (20), as well as the linearization of the nonlinear constraints specified in equation (21).

$$\min_{\boldsymbol{p} \in \mathbb{R}^m} \quad \frac{1}{2} \boldsymbol{p}^T \boldsymbol{H}_k \boldsymbol{p} + \nabla \mathrm{f}(\boldsymbol{x}_k)^T \boldsymbol{p} \qquad (21a)$$

$$\text{s.t.} \quad \nabla g_i(\boldsymbol{x}_k)^T \boldsymbol{p} + g_i(\boldsymbol{x}_k) = 0, \ \forall\ i \in \mathbf{I} \qquad (21b)$$

$$\nabla g_j(\boldsymbol{x}_k)^T \boldsymbol{p} + g_j(\boldsymbol{x}_k) \le 0, \ \forall\ j \in \mathbf{J} \qquad (21c)$$

where $\boldsymbol{p}$ represents the search direction originating from the QP subproblem and $\mathbf{H}_k$ denotes the Hessian matrix derived from Eq. (20).

Subsequently, the solution to the QP subproblem, denoted as $\boldsymbol{p}_k$, is utilized to generate a new iterate $\boldsymbol{x}^{k+1} := \boldsymbol{x}^k + \alpha_k \boldsymbol{p}_k$. The determination of the appropriate step size α_k is crucial to ensure a significant reduction in a merit function, which measures the quality of the solution obtained during each iteration.

2) MPC using successive linearization (MPC-SL): In the MPC-SL method, a linear time-varying (LTV) model is utilized, derived through successive linearization in the prediction model. This method performs *"online linearization"* in each iteration, based on the current operational points. The prediction model, covering a span of N_p, is integrated into (15) to determine optimal control actions for the nonlinear controlled system. The formulation of MPC-SL is referenced in [34], [35]. Two main steps should be applied for this method:

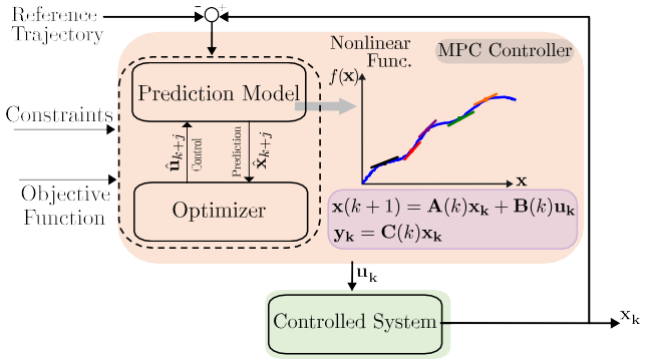

Fig. 5. Schematic diagram of the MPC controller using successive linearization.

(1) The state-space representation for the MG is formulated using a linear approximation of the predicted continuous nonlinear system dynamics.

Remark. *The model is first linearized offline, based on its operating points. Subsequently, for the implementation of MPC-SL, the system dynamics are linearized at each specific time instant* k *around the operating points.*

(2) The continuous state-space representation of the system will be discretized. This process transforms the system into a discrete-time model, expressible as $\boldsymbol{x}(k+1) = \mathbf{A}(k)\boldsymbol{x}(k) + \mathbf{B}(k)\boldsymbol{u}(k)$.

During the MPC-SL implementation, steps (1) and (2), are repeatedly conducted by linearizing the system around the

Authorized licensed use limited to: LEHIGH UNIVERSITY. Downloaded on June 09,2024 at 16:25:19 UTC from IEEE Xplore. Restrictions apply.
© 2024 IEEE. Personal use is permitted, but republication/redistribution requires IEEE permission. See https://www.ieee.org/publications/rights/index.html for more information.

This article has been accepted for publication in IEEE Transactions on Energy Conversion. This is the author's version which has not been fully edited and content may change prior to final publication. Citation information: DOI 10.1109/TEC.2024.3365353

measurement of the current states and the previous control inputs $(\boldsymbol{x}_0|\mathrm{k}, \boldsymbol{u}_0|\mathrm{k})$ for all $\mathrm{k} \in \{0, \ldots, \mathrm{T}-1\}$ (Fig. 5). Hence, the prediction model is expressed as follows:

$$\boldsymbol{x}(\mathrm{k}+\mathrm{j}) = \mathbf{A}^{j}(\mathrm{k})\boldsymbol{x}(\mathrm{k}) + \sum_{i=0}^{j-1} \mathbf{A}^{i}(\mathrm{k})\mathbf{B}(\mathrm{k})\boldsymbol{u}(\mathrm{k}+\mathrm{i}) + (\boldsymbol{I}+\mathbf{A}(\mathrm{k}))^{j-1}\boldsymbol{\Gamma}(\mathbf{k}) \quad \forall\ \mathrm{j} \in \{1, \ldots, \mathrm{N}_p\} \tag{22}$$

where $\mathbf{A}^{j}(\mathrm{k}) \in \mathbb{R}^{N_p n_x \times n_x}$ signifies the time-varying prediction matrix linked with current states measurement, $\sum_{i=0}^{j-1} \mathbf{A}^{i}(\mathrm{k})\mathbf{B}(\mathrm{k}) \in \mathbb{R}^{N_p n_x \times N_p(n_x+n_u)}$ corresponds to the time-varying prediction matrix associated to the control sequence, and $(\boldsymbol{I} + \mathbf{A}(\mathrm{k}))^{j-1} \in \mathbb{R}^{N_p n_x \times n_x}$ represents the prediction matrix of the affine term stemming from linearization.

V. Simulation Results

To assess and verify the applicability of the proposed SRc-based NLMPC approach for MG control, a representative MG system as depicted in Fig. 1 (plant side) is employed. The model is initially learned from available data and subsequently utilized in control optimization using NLMPC. In this section, five scenarios are conducted to evaluate the effectiveness of SRc-based NLMPC.

A. Impact of Sparsity Parameter (η)

In SR, the sparsity parameter (η) regulates model sparsity, controlling the number of non-zero coefficients in the coefficient matrix ($\boldsymbol{\Xi}$) that represents dynamics. Optimal η balances complexity and accuracy, preventing underfitting or overfitting. As a consequence, choosing an appropriate value for η is crucial in balancing model complexity and accuracy. In this scenario, two distinct values of the sparsity parameter were examined. Through a comprehensive analysis, it was determined that for the DER model, $\eta = 0.0001$ yielded more accurate results, as depicted in Fig. 6.

B. SR Accuracy Validation

The objective of this scenario is to evaluate the effectiveness of SR on identifying MG dynamics. The model is trained on a subset of the data (training set) and then evaluated on the remaining subset (validation set). The aim is to assess how well SR performs under different excitation conditions (on unseen or new data) in the control signal. Fig. 7, illustrates the training phase of the model, subjected to constant inputs and sinusoidal excitation, with a simulation time-step (s_p) of 0.0001 seconds. This corresponds to a training duration of 0.5 seconds, yielding 50,000 samples. In the subsequent validation phase, which also spans 0.5 seconds, the model is tested against variable step references. The results in Fig. 7, illustrate that the proposed SR approach accurately identifies the nonlinear and linear dynamics of the DER. The achieved MAPE stands at 0.38 % for the exemplary parameter θ, while for the primary state (ΔP_V) of the diesel generator, the MAPE becomes 1.03 %. This outcome underscores the effectiveness of the proposed SR technique in capturing the dynamics of the DER components.

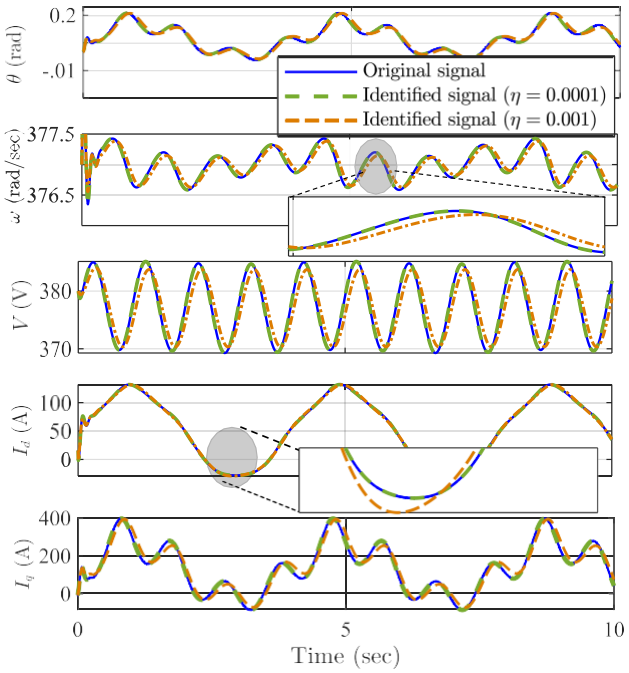

Fig. 6. Impact of sparsity parameter on model identification.

C. Adaptive SR method for Retraining After Parameter Changes

Fig. 8 illustrates the effectiveness of retraining the SR for system identification during parameter changes, without changing the candidate function matrix $\boldsymbol{\Theta}$ and the regularization parameter η.

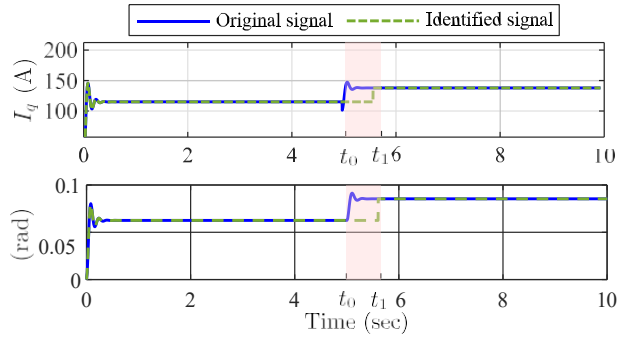

Fig. 8. Adaptive SR validation for retraining after parameter change.

The figure captures the critical moments for model retraining, specifically when divergences are observed between the estimated (identified signal) and actual measurements (original signal) in the time interval from t_0 to t_1. Despite the parameter changes, the SR model is promptly retrained with the same $\boldsymbol{\Theta}$ and η, which allows for a rapid realignment of the model parameters to accurately match the current dynamics of the system. This quick re-adaptation underscores the robustness of the SR model and its capacity to maintain precise system identification even in the face of changing system conditions. The effectiveness of this approach without the need to alter $\boldsymbol{\Theta}$ and η during retraining is a testament to the resilience of the

Authorized licensed use limited to: LEHIGH UNIVERSITY. Downloaded on June 09,2024 at 16:25:19 UTC from IEEE Xplore. Restrictions apply.
© 2024 IEEE. Personal use is permitted, but republication/redistribution requires IEEE permission. See https://www.ieee.org/publications/rights/index.html for more information.

This article has been accepted for publication in IEEE Transactions on Energy Conversion. This is the author's version which has not been fully edited and content may change prior to final publication. Citation information: DOI 10.1109/TEC.2024.3365353

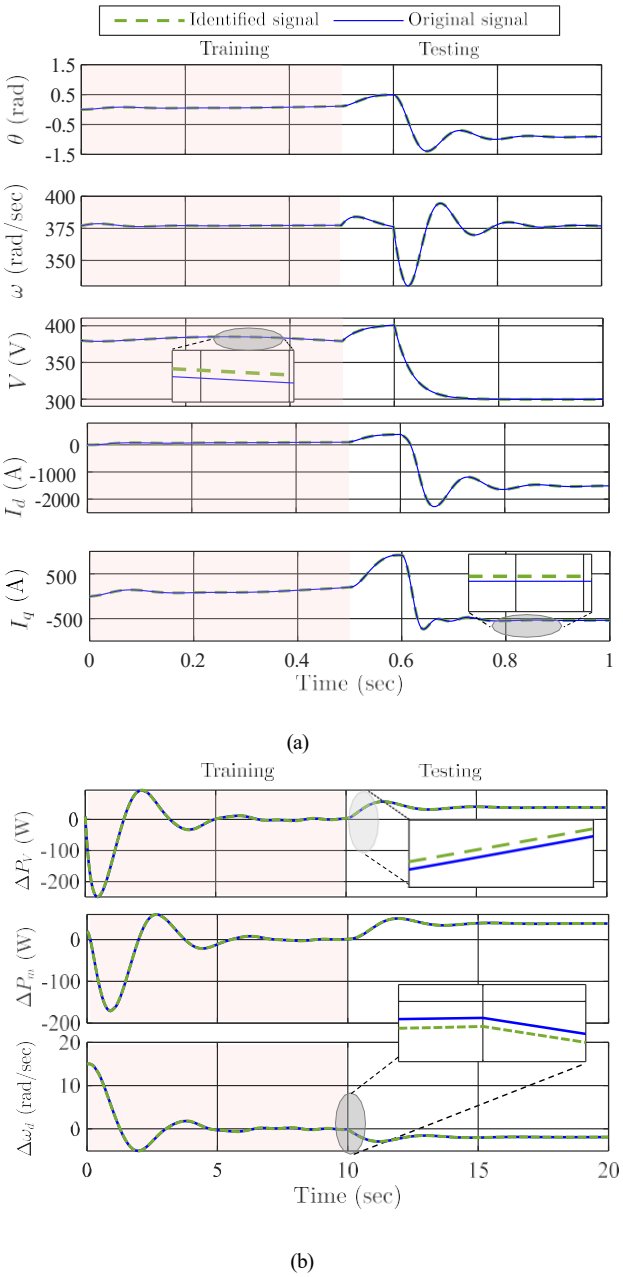

Fig. 7. Comparative analysis of time Series data for training and testing validation of a) DER and b) diesel generator performance based on SR accuracy.

Table III. Resistor Parameter change in the DER.

Parameter	Time (s)	Value (Ω)
R	$0 < t \leq 5$	160×10^{-3}
	$5 < t \leq 10$	200×10^{-3}

model's initial configuration. Algorithm 3 provides a detailed description of the retraining process used in this method.

D. Data-Driven Power Sharing Results Using NLMPC

To assess the efficacy of the proposed data-driven NLMPC controller, time-domain simulations are conducted on an islanded mode MG using the MATLAB Simscape power system toolbox. Assuming full observability of states ($\boldsymbol{x}$), the control

Algorithm 3: Adaptive SR Method Algorithm with Divergence Time Identification

Data: Initial Data
Result: Retrain Model
Output: Divergence Times: t_0, t_1
Collect initial data
Find initial model
$t_0 \leftarrow$ None
$t_1 \leftarrow$ None
while *Process not finished* **do**
  Collect more data
  if *Current time is* t_0 **then**
    Mark t_0 as the beginning of divergence
  else if *Current time is* t_1 **then**
    Mark t_1 as the end of divergence
    if *Model diverged between* t_0 *and* t_1 **then**
      Update model to handle divergence
      $t_0 \leftarrow$ None
      $t_1 \leftarrow$ None
    end
  else if *Model diverged and* t_0, t_1*are None* **then**
    Update model to handle unexpected divergence
  end
  if t_0 *is not None and* t_1 *is None* **then**
    Continue collecting data to confirm end of divergence
  end
  Check if process is finished
end

of three DGs was implemented using NLMPC to achieve the desired active and reactive power levels (P_{load} and Q_{load}).

To achieve effective power sharing while maintaining voltage and frequency stability, it is essential to satisfy the power sharing among DGs. Furthermore, considering Equations (15) to (19), it is necessary to optimally control the set-points of voltage and frequency for the two DERs (represented by inputs u_2, u_1 for DER 1, and u_4, u_3 for DER 2, respectively) in order to meet the specified reference points for P_{load} and Q_{load} presented in Table IV, as shown if Fig. 9a. By generating these optimal control actions by NLMPC, the terminal voltage and frequency of the inverters (represented by states x_2, x_3 for inverter 1, and x_7, x_8 for inverter 2, respectively) are maintained at desired levels, previously explained in subsection II.C, and it is presented in Fig. 9b, enabling efficient power sharing among the DERs. Moreover, Fig. 9b presents an insightful comparison between data-driven NLMPC and physics-based NLMPC, highlighting their striking similarity and validating our model-free control approach.

Based on the analysis presented in Fig. 10, the allocation of active and reactive power generation among all DERs is achieved through the implementation of optimal control actions generated by the NLMPC algorithm. Additionally, in order to provide a clear demonstration of the adherence of DERs to their assigned distribution allocation coefficients (calculated in section II.C), which is one of the objectives of the NLMPC

Authorized licensed use limited to: LEHIGH UNIVERSITY. Downloaded on June 09,2024 at 16:25:19 UTC from IEEE Xplore. Restrictions apply.
© 2024 IEEE. Personal use is permitted, but republication/redistribution requires IEEE permission. See https://www.ieee.org/publications/rights/index.html for more information.

This article has been accepted for publication in IEEE Transactions on Energy Conversion. This is the author's version which has not been fully edited and content may change prior to final publication. Citation information: DOI 10.1109/TEC.2024.3365353

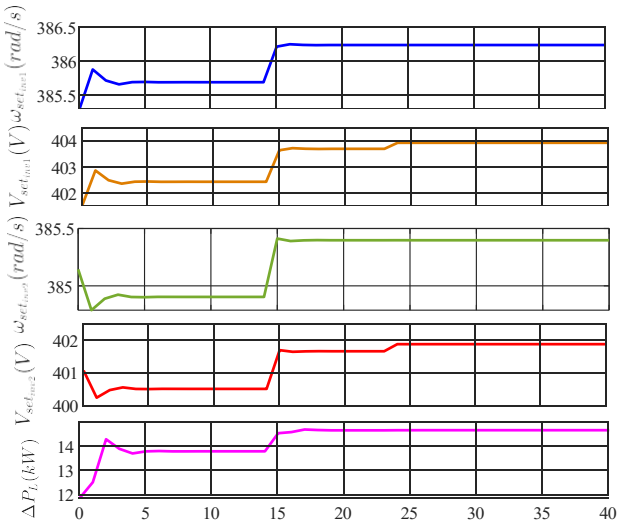

(a) Optimal control actions by NLMPC.

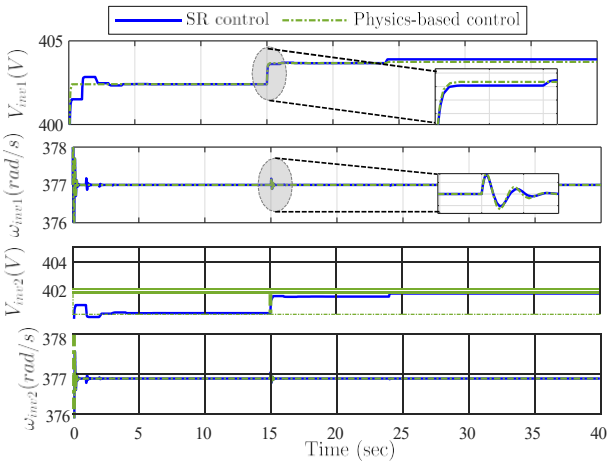

(b) Output voltage and frequency of DERs.

Fig. 9. NLMPC control actions and outputs.

algorithm, Fig. 11 is presented. The figure consists of three subplots, each representing a different droop coefficient: $\alpha = 1.1$ in the first subplot, $\beta = 5.8$ in the second subplot, and $\gamma = 1.08$ in the last subplot. This figure depicts the relationship between the generated power and the corresponding frequency deviation, highlighting the effectiveness of the control strategy in maintaining the desired droop characteristics of the DERs. Fig. 12 presents the state trajectories of each DER, providing a representation of their tracking performance. The trajectory plots demonstrate the ability of all DERs to closely follow the reference active power as evidenced by MAPE $= 3.46\%$, which is set equal to the active power of the load, as well as the reference reactive power, which corresponds to the reactive power of the load with MAPE $= 1.48\%$. This successful tracking performance is consistent with the values provided in Table IV.

E. Data-Driven Power Sharing Results Using NLMPC Under Real-world Load Pattern Scenario

In this section, we utilize a normalized real-world load pattern obtained from [36] to evaluate the performance of

Table IV. Reference points

Parameter	Time (s)	Values	Units
$P_{\text{ref}} = P_{\text{load}}$	$0 < t \leq 15$	160	kW
	$15 < t \leq 40$	170	
$Q_{\text{ref}} = Q_{\text{load}}$	$0 < t \leq 24$	15	kVAR
	$24 < t \leq 40$	18	

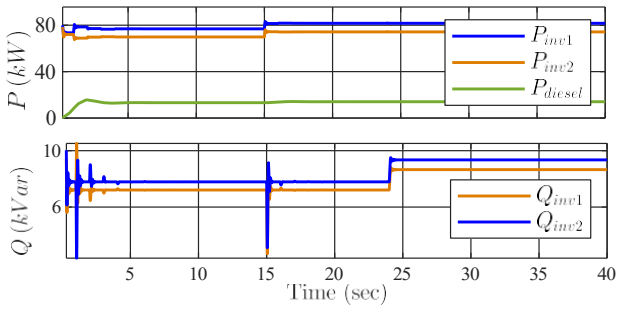

Fig. 10. Active and reactive power sharing among DERs.

the NLMPC algorithm. The load pattern, obtained from the Northwest region of China on December 3rd, 2018, represents the variations in P_{load} and Q_{load} over a 24-hour period. Fig. 13 illustrates the control actions generated by the NLMPC algorithm in response to the uncertain load pattern. Despite the presence of load uncertainties, the system successfully adheres to the permissible voltage and frequency boundaries, as depicted in Fig. 14. This demonstrates the effective performance of the NLMPC algorithm in regulating the MG operation under uncertain load conditions. The DERs are able to track the reference trajectories as shown in Fig. 15, indicating the accurate and reliable performance of the NLMPC algorithm in achieving the desired power sharing objectives with MAPE $= 5.19\%$ for active power and MAPE $= 1.75\%$ for reactive power. Overall, the results provide empirical evidence of the effectiveness of the NLMPC algorithm in regulating the operation of the MG, even in the presence of uncertain load patterns.

Fig. 16 depicts the time delay across 15 iterations (each iteration is a complete solution of NLMPC), evidencing the NLMPC algorithm's steadfast adherence to the demands of real-time operation. Execution times per control step exhibited minimal variation, with the average around 0.012 seconds, well within the system's 0.001 sample time. This indicates the

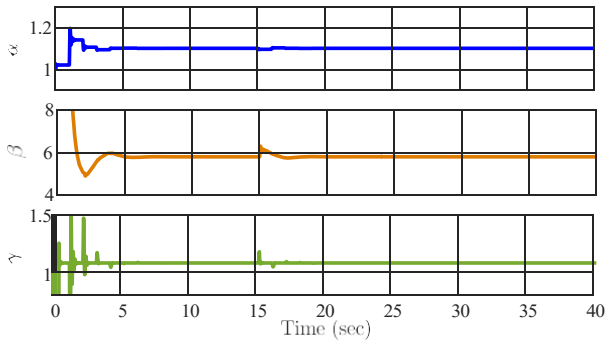

Fig. 11. Power sharing allocation based on droop gain calculation.

Authorized licensed use limited to: LEHIGH UNIVERSITY. Downloaded on June 09,2024 at 16:25:19 UTC from IEEE Xplore. Restrictions apply.
© 2024 IEEE. Personal use is permitted, but republication/redistribution requires IEEE permission. See https://www.ieee.org/publications/rights/index.html for more information.

This article has been accepted for publication in IEEE Transactions on Energy Conversion. This is the author's version which has not been fully edited and content may change prior to final publication. Citation information: DOI 10.1109/TEC.2024.3365353

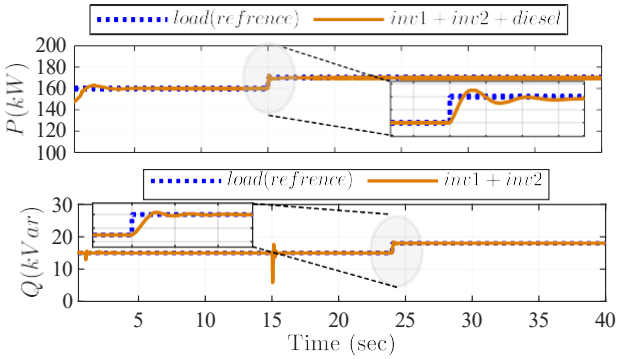

Fig. 12. Active and reactive Power load demand fulfilment.

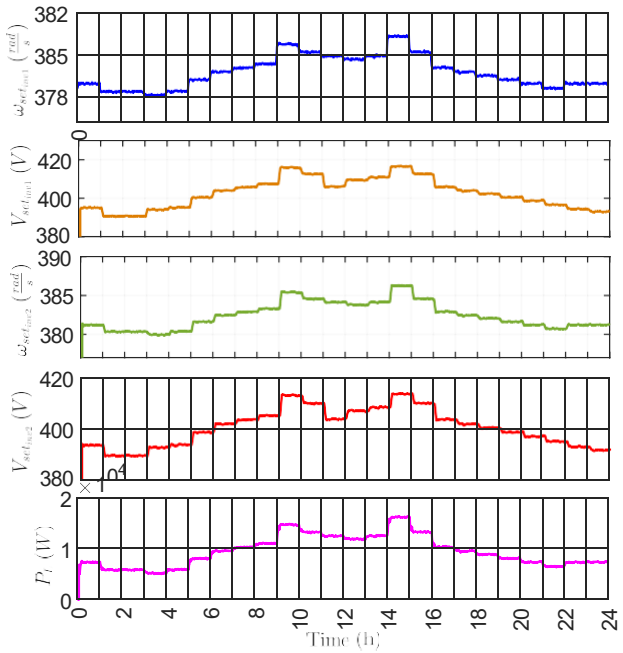

Fig. 13. Optimal control actions by NLMPC for real-world scenario.

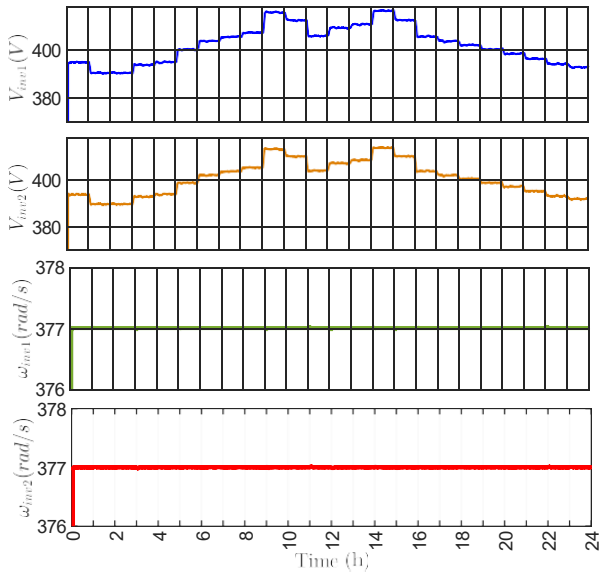

Fig. 14. Output voltage and frequency of DERs for real-world scenario.

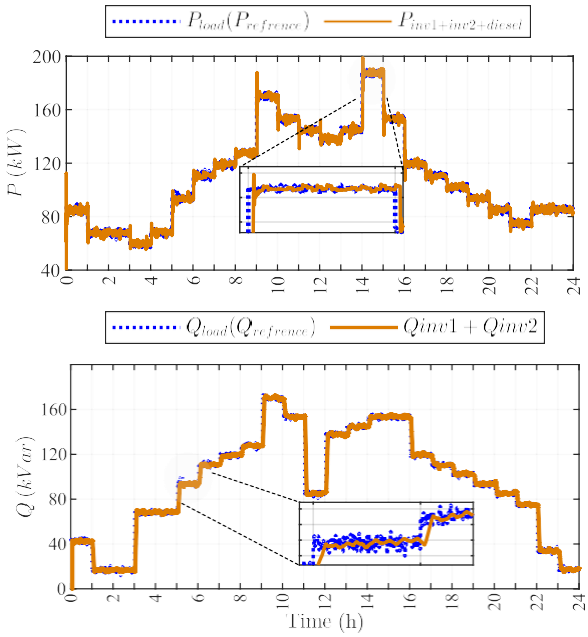

Fig. 15. Reference point tracking for real-world scenario.

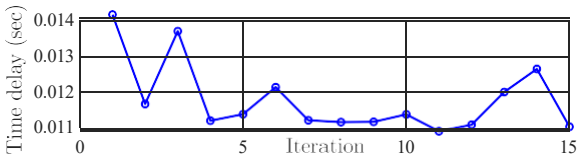

Fig. 16. Time delay of each NLMPC's solution.

algorithm's capacity to deliver optimal control actions expediently, capitalizing on the dynamic performance advantages of NLMPC.

F. Comparison between NLMPC and MPC-SL

Distinct comparison between NLMPC and MPC-SL methods is shown in Fig. 17. The system consists of two DERs. Within this system, the load profiles are dynamic; specifically, P_{load} exhibits a step change from 79 kW to 102 kW precisely at the t = 70 s, while Q_{load} adjusts from 11.4 kVar to 10 kVar at t = 100 s. The analysis depicted in the figure highlights the NLMPC's substantial efficacy over MPC-SL in adhering to the reference trajectory for both real and reactive power. Furthermore, NLMPC's capability to regulate transient responses—characterized by its attenuated overshoot and undershoot phenomena—is notably pronounced when the system encounters abrupt changes in reference values. This robust control is essential for maintaining system stability and ensuring seamless power sharing in MG. Furthermore, Table V also presents a comparison of the computational time required for each MPC solution, where it can be observed that NLMPC, despite its enhanced precision, requires only a marginally higher computational time compared to MPC-SL, underscoring its efficiency in complex control scenarios.

Authorized licensed use limited to: LEHIGH UNIVERSITY. Downloaded on June 09,2024 at 16:25:19 UTC from IEEE Xplore. Restrictions apply.
© 2024 IEEE. Personal use is permitted, but republication/redistribution requires IEEE permission. See https://www.ieee.org/publications/rights/index.html for more information.

This article has been accepted for publication in IEEE Transactions on Energy Conversion. This is the author's version which has not been fully edited and content may change prior to final publication. Citation information: DOI 10.1109/TEC.2024.3365353

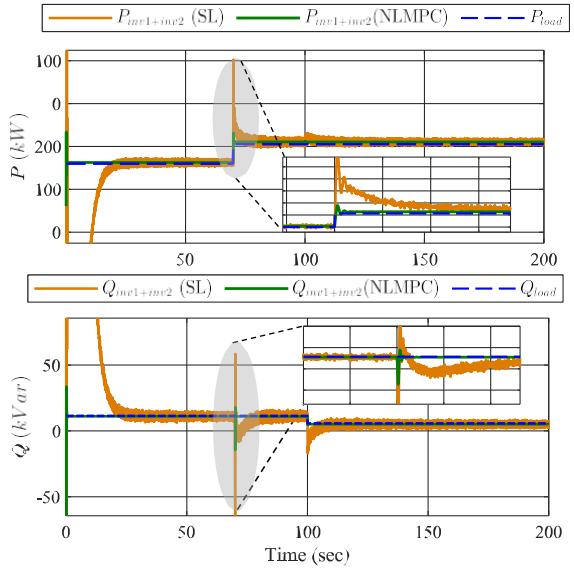

Fig. 17. Comparison between MPC using SL and NLMPC.

Table V. Quantitative Performance of MPC-SL and NLMPC

	MPC-SL	NLMPC
Each time solution of MPC (sec)	0.008	0.012
MAPE of P_{ref} tracking (%)	71.22	6.83
MAPE of Q_{ref} tracking (%)	63.10	5.71

VI. Stability Analysis

A fundamental requirement for the reliable operation of control systems is the establishment of bounded-input bounded-output (BIBO) stability. For a given system, BIBO stability is attained if, for every input function $\boldsymbol{u}(t)$ that is bounded by a finite scalar M_u, i.e., $\sup_{t\in\mathbb{T}} |\boldsymbol{u}(t)| \leq M_u$, the resulting output function $\boldsymbol{y}(t)$ also remains bounded within a finite scalar M_y, such that $\sup_{t\in\mathbb{T}} |\boldsymbol{y}(t)| \leq M_y$. Here, $\mathbb{T}$ signifies the time domain over which the system is analyzed. In the context of nonlinear dynamics, represented by Equation (3), BIBO stability necessitates the existence of a bounding function $g : \mathbb{R} \to \mathbb{R}$, ensuring $|f(\boldsymbol{u}(t))| \leq g(\sup_{t\in\mathbb{T}} |\boldsymbol{u}(t)|)$, and is subject to g being finite for all $\|\boldsymbol{u}\|_{L^\infty(T)} \leq M_u$. This can be further formalized through the employment of Lebesgue integrals within an L^p space, thereby defining $\|f(\boldsymbol{u})\|_{L^p(T)} \leq G(\|\boldsymbol{u}\|_{L^\infty(T)})$, where G is a monotonically non-decreasing function that correlates the supremum norm of the input to the L^p-norm of the output.

To ensure the stability of a nonlinear inverter model, we linearize it for eigenvalue analysis, as shown in the pole map (Fig. 18), which illustrates the effect of parameter R on stability. Poles λ_1 and λ_2 are located in the left half-plane, indicating stable behavior; however, their positions are significantly influenced by variations in the resistance R. This implies that the stability of the system can be compromised by these two poles as the value of R changes, particularly at $R = 200e^{-3}\Omega$. Meanwhile, poles λ_3, λ_4, and λ_5 near the imaginary axis highlight a variable stability margin. In parallel, NLMPC controllers enhance robustness by preemptively constraining system outputs and inputs, as per Equations (18) and (17). This predictive approach, essential for BIBO stability, adjusts

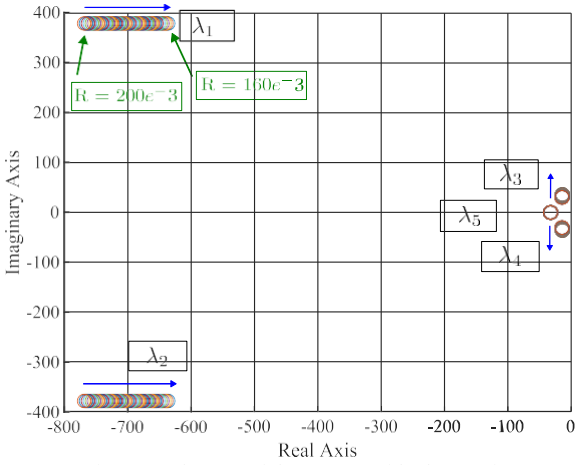

Fig. 18. Pole map of the system with changes in R.

control inputs $\boldsymbol{u}$ within set bounds to maintain output $\boldsymbol{y}(t)$ stability, corroborated by the pole map analysis.

VII. Real-time Verification

In discrete-time simulations, system states depend on previous time step values. Offline simulations aim to obtain results as quickly as possible based on the computer power and complexity of the model. Conversely, real-time simulations require accurate system representation. To be valid, a real-time simulation must replicate the system's variables and outputs in the same time as the actual system. The computation for each time step should be shorter than its real duration, allowing the simulator to manage operations like I/O for connected devices, ensuring simulation relevance [37].

This section involves real-time implementation of data-driven active and reactive power tracking, showed in Section V.D, using NLMPC on the OPAL-RT testbed shown in Fig. 20. The DERs with NLMPC control is first built in Simulink® and compiled with RT-LAB. This model then operates on an OP4510 real-time target CPU core. Control is managed via a TCP/IP connection from the Simulink® GUI on the main computer. Finally, we ensure that desired measurements are relayed in real-time to a digital oscilloscope, utilizing the analog outputs of the OP4510 target.

Fig. 19 illustrates that the real-time waveforms for the reference tracking of P and Q using the SR NLMPC controller are in tight agreement with their pre-simulated equivalents depicted in Fig. 12. The real-time trajectories for P_{DERs} and Q_{DERs} (indicated by the blue curve) closely match those for P_{load} and Q_{load} (indicated by the red curve), demonstrating a high degree of correlation. This observation validates the SR NLMPC controller's capability for precise real-time application.

VIII. Conclusion

This study highlights the effectiveness of the SR-based NLMPC framework for identifying and controlling nonlinear dynamics in MGs for the purpose of power sharing. By employing the SR technique known as SR, the nonlinear dynamics of a 3-DER MG were accurately captured. These dynamics were then integrated into the NLMPC framework,

Authorized licensed use limited to: LEHIGH UNIVERSITY. Downloaded on June 09,2024 at 16:25:19 UTC from IEEE Xplore. Restrictions apply.
© 2024 IEEE. Personal use is permitted, but republication/redistribution requires IEEE permission. See https://www.ieee.org/publications/rights/index.html for more information.

This article has been accepted for publication in IEEE Transactions on Energy Conversion. This is the author's version which has not been fully edited and content may change prior to final publication. Citation information: DOI 10.1109/TEC.2024.3365353

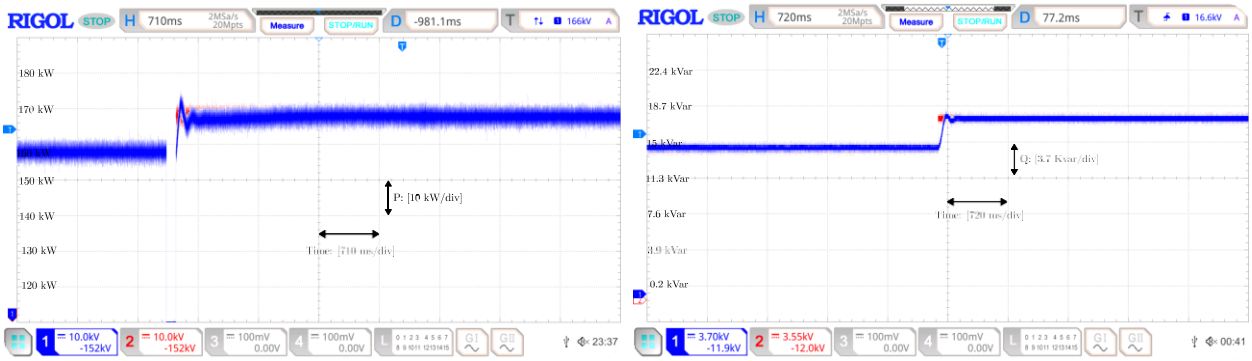

Fig. 19. Validating active and reactive power tracking of NLMPC for the section V.D in Real-time simulation setup.

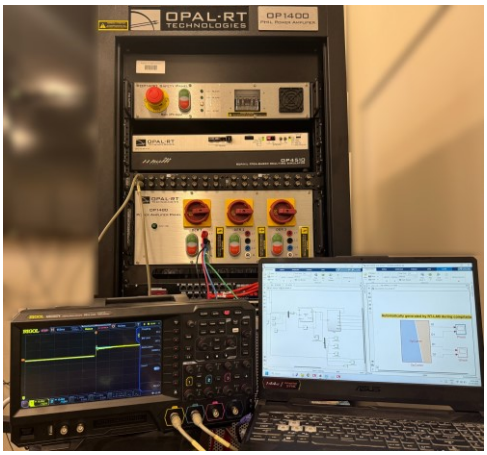

Fig. 20. Real-time simulation setup.

Table VI. Parameters of 3-DER MG.

DER	P_{min}	P_{max}	Q_{min}	Q_{max}
Inverter 1	0	90	0	13.5
Inverter 2	0	100	0	15
Diesel generator	0	500	N/A	N/A

DER	K_p	K_q
Inverter 1	7×10^{-6}	2.8×10^{-3}
Inverter 2	6.3×10^{-6}	2.58×10^{-3}
Diesel generator	1.2×10^{-6}	N/A

Parameter	Description	Value
S_n	Nominal DER Apparent Power	10 kVA
V_0	Nominal Peak Phase Voltage	380 V
ω_0	Nominal Frequency	377 rad/s
L_c	Coupling Inductance	0.15 mH
R_c	Coupling Resistance	25 mΩ
ω_c	Filter Constant	31.4 rad/s/W
L_l	Line Inductance	0.11 mH km^{-1}
R_l	Line Resistance	140 mΩ km^{-1}
τ_T	Turbine Time Constant	0.5 sec
τ_g	Governor Time Constant	0.2 sec
H	Governor Inertia Constant	5 sec
C	Governor Speed Regulation	0.05 p.u.

resulting in guaranteed tracking performance and the ability to accommodate varying desired state values and constraints, such as power balance equations and droop gains. Moreover, when tested with real-world load patterns and considering load uncertainty, the proposed data-driven NLMPC approach showcased its resilience and suitability for practical MG applications with the MAPE = 5.19% for active power tracking and MAPE = 1.75% for reactive power tracking over 24 hour for real-world load pattern scenario. Also, it outperforms other MPC strategies that rely on successive linearization, with a MAPE of 6.83% for active power and 5.71% for reactive power. Hence, this study presents a promising approach that combines data-driven identification with NLMPC, offering accurate modeling and robust control for MGs.

A forthcoming objective is to validate the effectiveness of the proposed data-driven NLMPC for MG control in a hardware-in-the-loop setup. Additionally, a comparison between the proposed NLMPC controller and conventional droop controllers will be considered.

REFERENCES

[1] J. Yan, S. Chou, B. Chen, F. Sun, H. Jia, and J. Yang, "Clean, affordable and reliable energy systems for low carbon city transition," *Applied Energy*, vol. 194, pp. 305–309, 2017. [Online]. Available: https://www.sciencedirect.com/science/article/pii/S0306261917302982

[2] A. Bidram and A. Davoudi, "Hierarchical structure of microgrids control system," *IEEE Transactions on Smart Grid*, vol. 3, no. 4, pp. 1963–1976, 2012.

[3] N. Sharmila, K. Nataraj, and K. Rekha, "An efficient dynamic power management model for a stand-alone DC microgrid using CPIHC technique," *International Journal of Power Electronics and Drive Systems (IJPEDS)*, vol. 12, no. 3, pp. 1439–1439, 2021.

[4] U. K. Kalla, B. Singh, and S. S. Murthy, "Intelligent neural network-based controller for single-phase wind energy conversion system using two winding self-excited induction generator," *IEEE Transactions on Industrial Informatics*, vol. 12, no. 6, pp. 1986–1997, 2016.

[5] L. Djilali, E. N. Sanchez, F. Ornelas-Tellez, and M. Belkheiri, "Neural network based controller for an AC microgrid connected to a utility grid," in *2018 IEEE Latin American Conference on Computational Intelligence (LA-CCI)*, 2018, pp. 1–6.

[6] S. M. Mohiuddin and J. Qi, "Optimal distributed control of ac microgrids with coordinated voltage regulation and reactive power sharing," *IEEE Transactions on Smart Grid*, vol. 13, no. 3, pp. 1789–1800, 2022.

[7] Y. Shan, J. Hu, and H. Liu, "A holistic power management strategy of microgrids based on model predictive control and particle swarm optimization," *IEEE Transactions on Industrial Informatics*, vol. 18, no. 8, pp. 5115–5126, 2021.

[8] U. Tamrakar, T. M. Hansen, R. Tonkoski, and D. A. Copp, "Model predictive frequency control of low inertia microgrids," in *2019 IEEE 28th International Symposium on Industrial Electronics (ISIE)*. IEEE, 2019, pp. 2111–2116.

[9] M. S. Golsorkhi and D. D.-C. Lu, "A decentralized control method for islanded microgrids under unbalanced conditions," *IEEE Transactions*

Authorized licensed use limited to: LEHIGH UNIVERSITY. Downloaded on June 09,2024 at 16:25:19 UTC from IEEE Xplore. Restrictions apply.
© 2024 IEEE. Personal use is permitted, but republication/redistribution requires IEEE permission. See https://www.ieee.org/publications/rights/index.html for more information.

This article has been accepted for publication in IEEE Transactions on Energy Conversion. This is the author's version which has not been fully edited and content may change prior to final publication. Citation information: DOI 10.1109/TEC.2024.3365353

on Power Delivery, vol. 31, no. 3, pp. 1112–1121, 2015.
[10] A. Tavakoli, M. Negnevitsky, and K. M. Muttaqi, "A decentralized model predictive control for operation of multiple distributed generators in an islanded mode," *IEEE Transactions on Industry Applications*, vol. 53, no. 2, pp. 1466–1475, 2016.
[11] K. T. Tan, X. Peng, P. L. So, Y. C. Chu, and M. Z. Chen, "Centralized control for parallel operation of distributed generation inverters in microgrids," *IEEE Transactions on Smart Grid*, vol. 3, no. 4, pp. 1977–1987, 2012.
[12] F. Alonge, F. D'Ippolito, F. M. Raimondi, and S. Tumminaro, "Nonlinear modeling of DC/DC converters using the Hammerstein's approach," *IEEE transactions on power electronics*, vol. 22, no. 4, pp. 1210–1221, 2007.
[13] I. Cvetkovic, D. Boroyevich, P. Mattavelli, F. C. Lee, and D. Dong, "Non-linear, hybrid terminal behavioral modeling of a dc-based nanogrid system," in *2011 Twenty-Sixth Annual IEEE Applied Power Electronics Conference and Exposition (APEC)*. IEEE, 2011, pp. 1251–1258.
[14] G. Rojas-Duen˜as, J.-R. Riba, and M. Moreno-Eguilaz, "Black-box modeling of DC-DC converters based on wavelet convolutional neural networks," *IEEE Transactions on Instrumentation and Measurement*, vol. 70, pp. 1–9, 2021.
[15] A. Wunderlich and E. Santi, "Digital twin models of power electronic converters using dynamic neural networks," in *2021 IEEE Applied Power Electronics Conference and Exposition (APEC)*. IEEE, 2021, pp. 2369–2376.
[16] A. Wunderlich, K. Booth, and E. Santi, "Hybrid analytical and data-driven modeling techniques for digital twin applications," in *2021 IEEE Electric Ship Technologies Symposium (ESTS)*. IEEE, 2021, pp. 1–7.
[17] S. Zhao, Y. Peng, Y. Zhang, and H. Wang, "Parameter estimation of power electronic converters with physics-informed machine learning," *IEEE Transactions on Power Electronics*, vol. 37, no. 10, pp. 11 567–11 578, 2022.
[18] G. Kandaperumal, K. P. Schneider, and A. K. Srivastava, "A data-driven algorithm for enabling delay tolerance in resilient microgrid controls using dynamic mode decomposition," *IEEE Transactions on Smart Grid*, vol. 13, no. 4, pp. 2500–2510, 2022.
[19] Y. J. Isbeih, S. Ghosh, M. S. El Moursi, and E. F. El-Saadany, "Online DMDc based model identification approach for transient stability enhancement using wide area measurements," *IEEE Transactions on Power Systems*, vol. 36, no. 5, pp. 4884–4887, 2021.
[20] J. L. Proctor, S. L. Brunton, and J. N. Kutz, "Dynamic mode decomposition with control," *SIAM Journal on Applied Dynamical Systems*, vol. 15, no. 1, pp. 142–161, 2016.
[21] P. Karamanakos and T. Geyer, "Guidelines for the design of finite control set model predictive controllers," *IEEE Transactions on Power Electronics*, vol. 35, no. 7, pp. 7434–7450, 2020.
[22] A. Nurkanovic´, A. Mes˘anovic´, A. Zanelli, G. Frison, J. Frey, S. Albrecht, and M. Diehl, "Real-time nonlinear model predictive control for microgrid operation," in *2020 American Control Conference (ACC)*. IEEE, 2020, pp. 4989–4995.
[23] S. L. Brunton, J. L. Proctor, and J. N. Kutz, "Discovering governing equations from data by sparse identification of nonlinear dynamical systems," *Proceedings of the national academy of sciences*, vol. 113, no. 15, pp. 3932–3937, 2016.
[24] P. Vorobev, P.-H. Huang, M. Al Hosani, J. L. Kirtley, and K. Turitsyn, "High-fidelity model order reduction for microgrids stability assessment," *IEEE Transactions on Power Systems*, vol. 33, no. 1, pp. 874–887, 2017.
[25] H. Saadat, "Power system analysis, mcgrew-hill," *New York*, 1999.
[26] A. Yazdani and R. Iravani, *Voltage-sourced converters in power systems: modeling, control, and applications*. John Wiley & Sons, 2010.
[27] R. F. Mochamad, R. Preece, and K. N. Hasan, "Probabilistic multi-stability operational boundaries in power systems with high penetration of power electronics," *International Journal of Electrical Power & Energy Systems*, vol. 135, p. 107382, 2022.
[28] J. Khazaei, W. Liu, and F. Moazeni, "Data-driven sparse model identification of inverter-based resources for control in smart grids," in *2023 11th International Conference on Smart Grid (icSmartGrid)*. IEEE, 2023, pp. 1–6.
[29] M.-Q. Tran, T. T. Tran, P. H. Nguyen, and G. Pemen, "Sparse identification for model predictive control to support long-term voltage stability," *IET Generation, Transmission & Distribution*, vol. 17, no. 1, pp. 39–51, 2023.
[30] L. Zhang and H. Schaeffer, "On the convergence of the SINDy algorithm," *Multiscale Modeling & Simulation*, vol. 17, no. 3, pp. 948–972, 2019.
[31] E. F. Camacho and C. B. Alba, *Model predictive control*. Springer science & business media, 2013.
[32] R. Soeterboek, *Predictive control: a unified approach*. Prentice-Hall, Inc., 1992.
[33] J. Nocedal and S. J. Wright, *Numerical optimization*. Springer, 1999.
[34] A´ . Domina and V. Tihanyi, "LTV-MPC approach for automated vehicle path following at the limit of handling," *Sensors*, vol. 22, no. 15, p. 5807, 2022.
[35] M. H. Murillo, A. C. Limache, P. S. Rojas Fredini, and L. L. Giovanini, "Generalized nonlinear optimal predictive control using iterative state-space trajectories: Applications to autonomous flight of uavs," *International Journal of Control, Automation and Systems*, vol. 13, pp. 361–370, 2015.
[36] J. Qin, Y. Zhang, S. Fan, X. Hu, Y. Huang, Z. Lu, and Y. Liu, "Multi-task short-term reactive and active load forecasting method based on attention-LSTM model," *International Journal of Electrical Power & Energy Systems*, vol. 135, p. 107517, 2022.
[37] J. Be´langer, P. Venne, and J.-N. Paquin, "The what, where and why of real-time simulation," *Planet Rt*, vol. 1, no. 1, pp. 25–29, 2010.

Maral Shadaei (SM'21) was in the R&D department of Fars Power Maintenance Company in Shiraz, Iran, where she focused on innovative solutions for power system reliability and protection from 2019 to 2022. Currently she is pursuing a Ph.D. in electrical engineering at the Electrical and Computer Engineering Department at Lehigh University, PA, USA. Her research interests include data-driven modeling and control of modern power systems and microgrids.

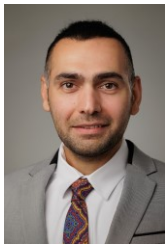

Javad Khazaei (S'10 M'16 SM'20) received the Ph.D. degree in Electrical Engineering from University of South Florida (USF) in 2016 with focus on power and energy systems. He is currently an Assistant Professor at the Electrical and Computer Engineering Department at Lehigh University, PA, USA. His research interests include data-driven and model-based control, optimization, and dynamic modeling of cyber-physical power systems and microgrids, smart grid security, and power electronics applications in smart grids and shipboard microgrids.

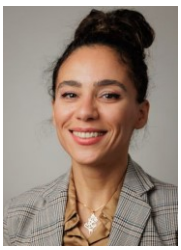

Faegheh Moazeni (M'23, AM (ASCE) '18) received the Ph.D. degree in Civil and Environmental Engineering from University of Nevada Las Vegas (UNLV) in 2013. She is currently an assistant professor of Civil and Environmental Engineering Department at Lehigh University. Her research interests include data-driven modeling and control with applications in smart water systems, water-energy nexus, and water system security against cyberattacks.

Authorized licensed use limited to: LEHIGH UNIVERSITY. Downloaded on June 09,2024 at 16:25:19 UTC from IEEE Xplore. Restrictions apply.
© 2024 IEEE. Personal use is permitted, but republication/redistribution requires IEEE permission. See https://www.ieee.org/publications/rights/index.html for more information.